Journal of Geoscience and Environment Protection, 2023, 11, 163-181
https://www.scirp.org/journal/gep
ISSN Online: 2327-4344
ISSN Print: 2327-4336

Petrographic Characteristics and Metalogeny of Zatua Hills BIFs, Haut-Uele Province (DR Congo)

Levesque Makuku Mbo[1,2,3*], Papy-Fidèle Kombie Andeibal[4], François Tshiabo Luwanda[2], Dominique Wetshondo Osomba[1,3], Valentin Kanda Nkula[1,2], Albert Ongendangenda Tienge[1]

[1]Department of Geosciences, Faculty of Science and Technology, University of Kinshasa, Kinshasa XI, DR Congo
[2]Geological and Mining Research Center (CRGM), Kinshasa, DR Congo
[3]Faculty of Oil, Gas and Renewable Energies, University of Kinshasa, Kinshasa XI, DR Congo
[4]Kinshasa, DR Congo
Email: *levmakuku@gmail.com

How to cite this paper: Mbo, L. M., Andeibal, P.-F. K., Luwanda, F. T., Osomba, D. W., Nkula, V. K., & Tienge, A. O. (2023). Petrographic Characteristics and Metalogeny of Zatua Hills BIFs, Haut-Uele Province (DR Congo). *Journal of Geoscience and Environment Protection, 11,* 163-181.
https://doi.org/10.4236/gep.2023.1112009

Received: November 18, 2023
Accepted: December 26, 2023
Published: December 29, 2023

Abstract

Zatua Hills are located at Haut Uélé Province of Democratic Republic of Congo (DRC), between northern Bafwasende and southern Paulis (Isiro) Squarred Degrees. Belonging to greenstone belt of Ngayu, that area is identified by the high elevated zone which is remained the witness of stable zone, not affected by the ancienst erosion process. Zatua Hills are in the superior Kibalian formation dated to Neoarchaen, hosted in Upper Congo Granites Massifs of DRC covering a large central zone of NE of DRC, and consisting to dolerite, phyllade, clay rich sediment, poor Banded Iron Formations (BIFs), enriched BIFs, friable hematite, hard hematite, mineralized and unmineralized brechias. Magnetite, martite and hematite are associated to some secondary minerals such as goethite, gibbsite, kaolinite, strengite, variscite and others clay minerals present in BIFs. Petrographic analysis made from the samples collected *in situ* showed, as well as BIFs and iron ore associated, that magnetite was much abundant oxide mineral which is oxided to martite before to stabilize to hematite during the deposition time. Having about hundred meters of thickness, the rich iron ore of this area content, in the majority less deleterious elements which, are harmful in metallurgic process of iron. These secondary minerals were precipitated at various degrees in the leached cavities of rocks between martite and hematite aggregates to botryoidal texture and, are rich to Al, and are mainly consisting to gibbsite and solid solution series of variscite-strengite ($AlPO_4{\cdot}2H_2O$ and $FePO_4{\cdot}2H_2O$). Low degree of metamorphism played when magnetite was converted to martite, with the presence of variscite and anatase like witnesses of this event in which, martite

was crystalized to hematite.

Keywords

BIFs, Zatua Hills, Petrographic, DRC, Iron Ore

1. Introduction

The Northeastern part of the DRC has immense iron resources that can reach tens or even hundreds of billions of tons, capable of initiating its industrialization policy and providing iron-based materials and alloys necessary for the needs of Central Africa, a potential market for road construction and civil engineering works. These resources are mainly related to the BIFs contained within the greenstone belt of the NE part of the DRC, including those of Ngayu, Zani, Kilo, Moto, Mambasa, Panga, Tele, and Isiro, which constitute the Kibalian series contained in most of the granitic massifs of the "Upper Congo Granites Complex," which are divided into an Early Kibalian, consisting of high grade metamorphic series, basaltic-type volcanic rocks, and tonalite intrusions (>2.8 Ga) with a scarcity of BIFs and metasediments (Lavreau, 1984). And a Late Kibalian, dominated by metasediments, large volumes of BIFs, rare volcanic rocks, and intruded by granitic rocks (>2.45 Ga) (Lavreau & Ledent, 1975; Lavreau, 1980). The main accumulations of these BIFs form high and very noticeable topography surfaces in the region, namely: the Tina, Maie, Asonga, Zatua Hills, etc.

In this publication, we focus on studying the BIFs of the Zatua Hills, characterized by a relatively smaller plateau with altitudes ranging from 500 to 1089 m. Chains and intermittent hills can rise up to 300 m above the surrounding plateau.

The target area consists of a serie of NW-SE trending hills, within which lies the Zatua Hills with a maximum elevation of 1300 m. To the southeast, the area is bordered by the Western Rift Valley, including Albert and Edward Lakes, separated by the Rwenzori Hills (5119 m).

Northeastern DRC occupies both the northeastern part of the Congo Basin and the elevated areas that constitute the western boundaries of the graben (rift) basin. This region, essentially composed of Archean shields, is covered by a series of Neoproterozoic and Phanerozoic formations that are affected by the aftershock of recent Cenozoic tectonic events that gave rise to the East African Rift.

This study presents the petrographic data from the various sites visited, with a focus on the metalogenic aspects and its significance for the quality of iron ore for metallurgical industries.

2. Study Area

2.1. Geographical Context

The Zatua Hills, which are the subject of this publication, are located between

the Bafwasende Degree Square in the north and the Isiro (Paulis) Degree Square in the south, and are situated between 27˚31'48" and 27˚40'48" East longitude and between 1˚55'48" and 2˚01'48" North latitude. They are located in the Wamba Territory, Haut-Uélé Province in the Democratic Republic of the Congo, approximately 315 km by air from the city of Kisangani (Figure 1).

This area is characterized by a relatively smaller plateau, with altitudes varying between 500 and 1089 m. Intermittent ranges and hills rise up to 300 m above the surrounding plateau.

The target area comprises a series of hills in a NW-SE direction, including the Zatua hills with a maximum altitude of 1300 m. To the south-east, the area is bordered by the Western Rift Valley, including Lakes Albert and Edouard, separated by the Ruwenzori massif (5119 m).

2.2. Geological Context

Regional geology is predominantly composed of the Archean-age basement formations covering an area of 500,000 km^2, including Uganda, South Sudan, and the Central African Republic (de Wit & Linol, 2015; Borg & Shackleton, 1997;

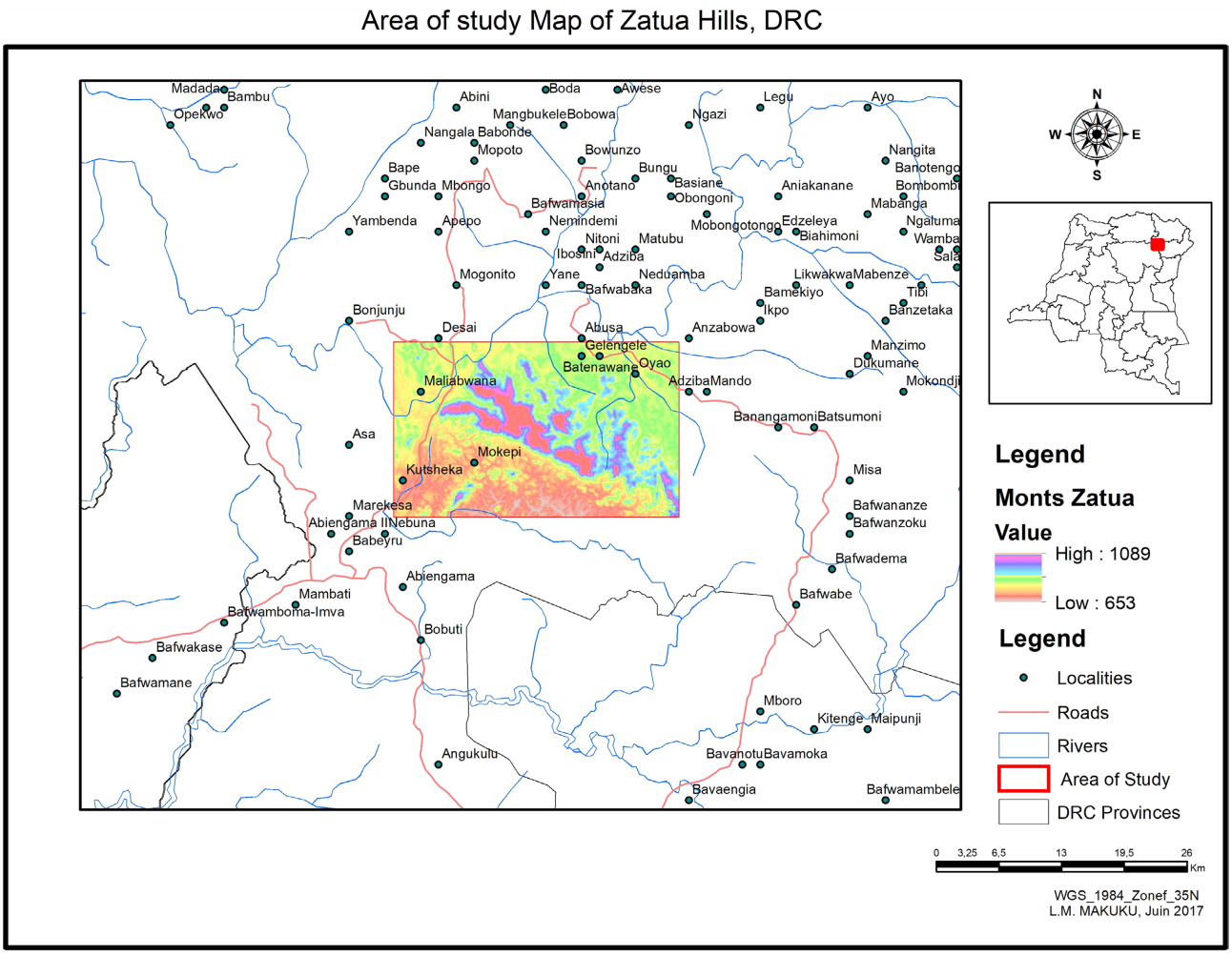

Figure 1. Location map of the study area (Makuku et al., 2023).

Cahen & Snelling, 1966). These formations were initially associated with the Tanzanian craton before being separated by the Ruwenzori chain (2 Ga) and the filling of rift basins (Borg & Shacklet, 1997; Lavreau & Navez, 1982). These formations include the Bomu amphibolitic and gneissic complex dated 3.4 - 3.7 Ga (Cahen et al., 1984), the West Nile amphibolitic complex dated 3200 - 2728 Ma (Allibone et al., 2020), the Garamba complex, the granitic massifs of the Upper Congo Granites Massifs, which cover a large part of the central area, consisting of magmatic, orthogneissic and various magmatic intrusions, in which the Kibalian greenstone belt formations, including BIFs, are associated, and which form the core of the large Archean units in the region (Lavreau, 1982; Cahen & Snelling, 1966; Lavreau, 1982; BRGM, 1982; Cahen et al., 1984; Bird, 2016; Allibone et al., 2020).

The Zatua Hills are part of the Ngayu belt, which is one of several greenstone belts found in the Nyanza-Kibali greenstone belt, which stretches from Tanzania to the Central African Republic.

The most remarkable formations in the region are the BIFs, which occupy vast stretches compared to other geological formations. Their presence is clearly shown on the map represented in **Figure 2**. These BIFs are considered as true

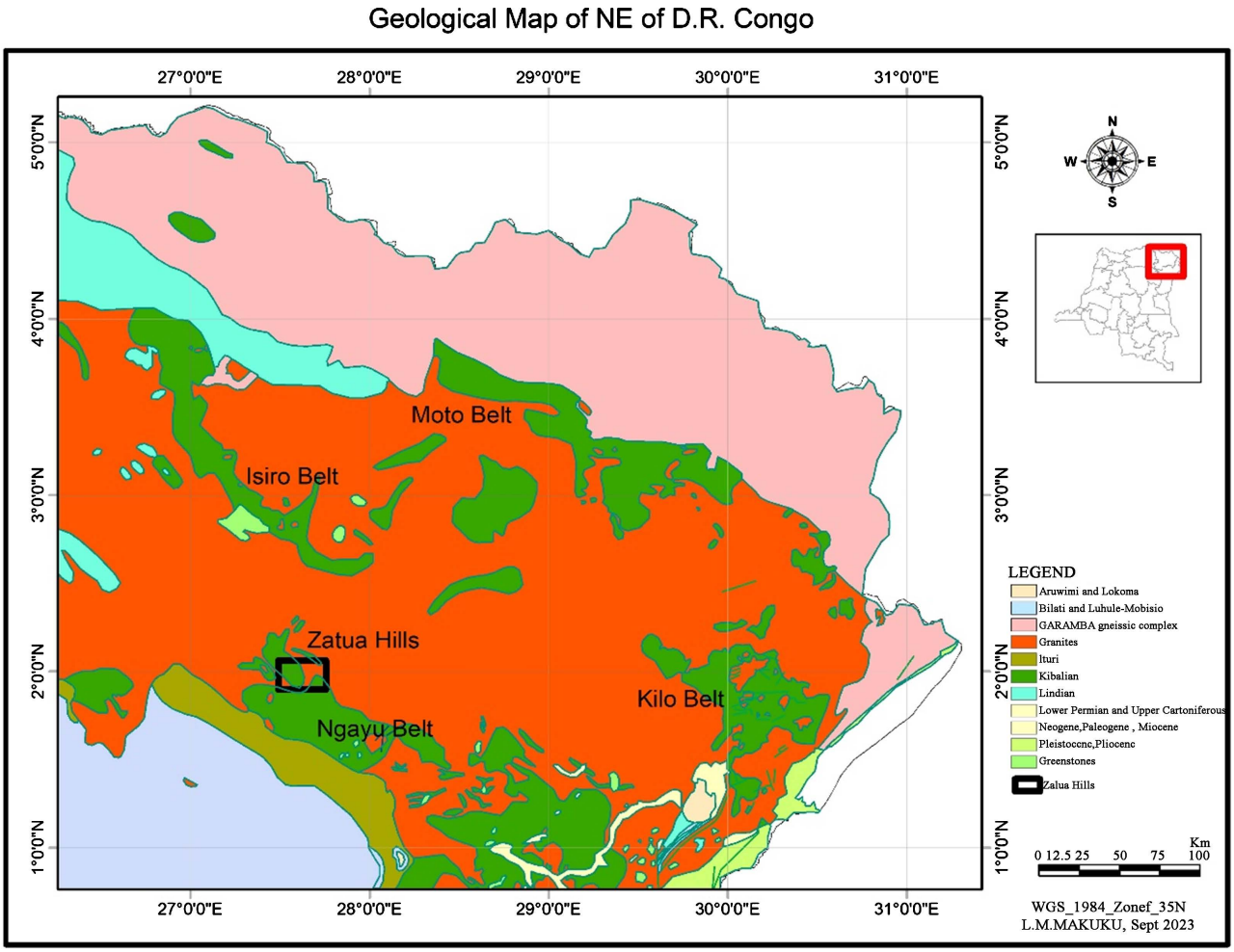

Figure 2. Geological map showing the different greenstone belts in which the BIFs of Zatua Hills are embedded (Allibone et al., 2020).

markers that define the different structural entities of the region. In some places, these formations can have significant thicknesses of up to 200 m, sometimes in association with certain deformations (folds, faults, laminations) and form relatively high reliefs. BIFs are sometimes found intercalated at the roof by schist rock and at the wall by basalts.

Apart from the BIFs, the region is also characterized by the presence of basaltic formations, intrusions of diorite, quartz monzonite and tonalite in greenstone rocks. All these rocks are covered by formations of Upper Proterozoic age (Lindian), Mesozoic formations and the West African Rift formations of Cenozoic age.

3. Methodology

This publication is the series of studies based on meticulous *in situ* observations, starting with multiple *in situ* outcrop mapping works, drilling works, petrographic analysis in the laboratory and metalogenic study based on results obtained both in the field and in the laboratory.

3.1. Field Stage

The work consisted of identifying the outcrop zones of BIFs, iron ores (enriched parts) and their host rocks using airborne magnetometric data acquired and interpreted by the company Rio Tinto, which once operated in this area, geological survey work on the relevant sites, collecting samples in the field, and mapping outcrop zones.

These data enabled the confirmation of zones with rich BIFs (% iron ≥ 50), poor BIFs (% iron < 50) and iron ores ((% iron ≥ 60), not forgetting the poor host rock ((% iron < 40).

Several samples were collected in these sites (**Figure 3**) and some were selected for petrography observations in the laboratory.

3.2. Lab Stage

The selected samples were used for petrographic observations in the laboratory, namely:

- Macroscopic analysis of the samples collected using the naked eye and a magnifying glass;
- Microscopic analyses using an optical microscope and a scanning electron microscope to examine iron oxides and post-depositional inclusions that could influence the quality of the iron ore encountered.

3.3. Interpretation and Discussion of Results Stage

The results of the petrographic analyses have enabled us to make a metalogenic interpretation of the Zatua Hills BIFs and the associated iron ores, while also taking a look at the associated elements that can influence the metallurgical quality of iron in its various stages through the formation of different alloys.

4. Results

The samples collected in the field were subjected to microscopic analysis using optical and scanning electron microscopes, the results of which are shown below:

4.1. Surface Samples

Of the 24 surface samples collected, we took care to select the petrographic analyses of 6 samples for the purposes of representativeness, details of which are given on the pages below (Figures 3-11).

4.1.1. Macroscopic Analysis

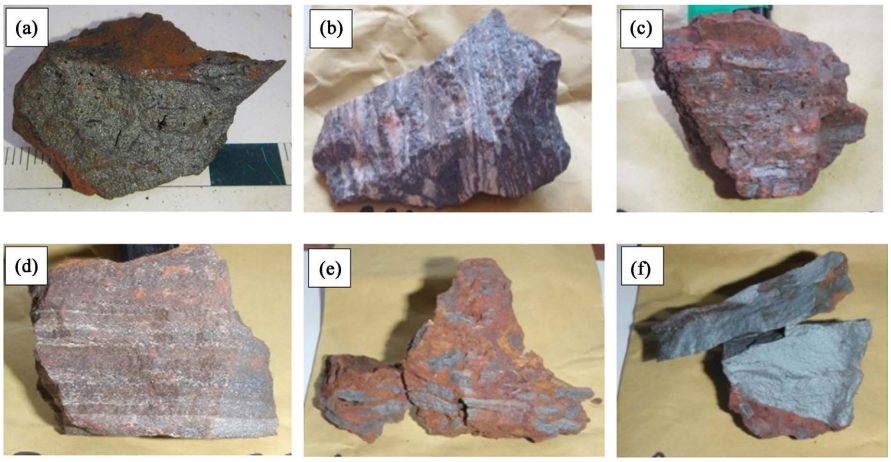

Figure 3. Outcrop samples of BIFs breccia (MZ002 in (a) and MZ017 in (e)), a rich iron ore or hematite (MZ022 in (c) and MZ024 in (f)) and BIFs (MZ004 in (d) and MZ008 in (b)).

4.1.2. Microscopic Analysis

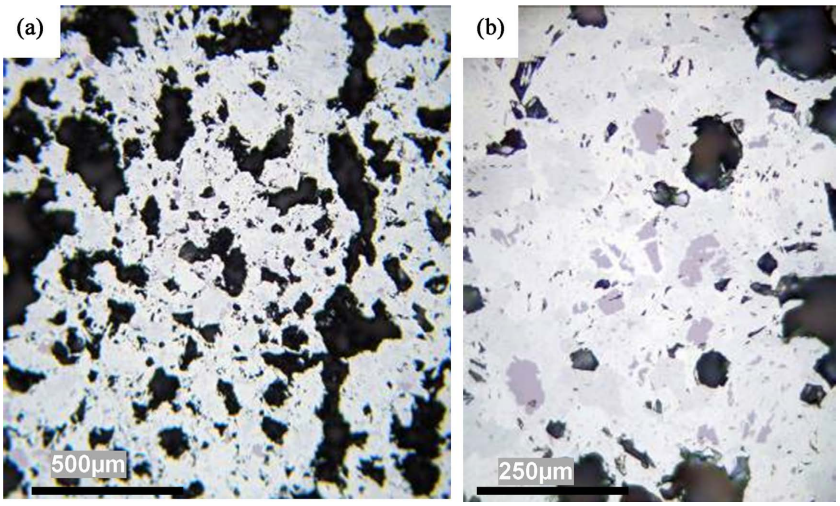

Figure 4. A reflected light microscope view of MZ002 showing (a) a portion of the magnetite-rich sample in which the pseudomorphic martite crystals (white) are cemented by the microplaty hematite crystals. The black part denotes pores or voids. In (b) a certain amount of residual unoxidised magnetite (pinkish grey) within a zone of partially recrystallized martite (whitish).

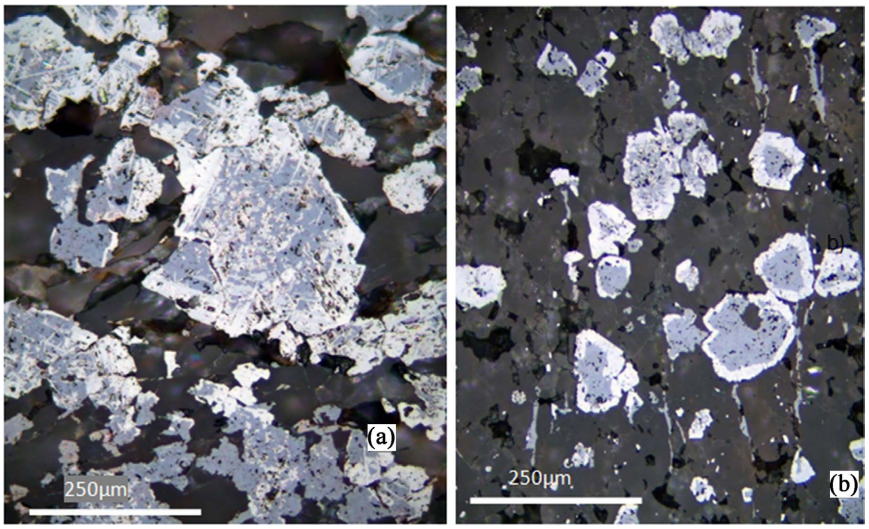

Figure 5. Reflected-light microscopy of MZ004 illustrating (a) the continuity of the replacement of martite (white) by goethite (grey). Note the presence of small crystals of lamellar and lattice martite within the goethite. In (b) the pseudomorphic martite after transformation of the magnetite by oxidation in which the interior of martite aggregates (in white) has been replaced by goethite (in grey). martite (in white) by goethite (in grey).

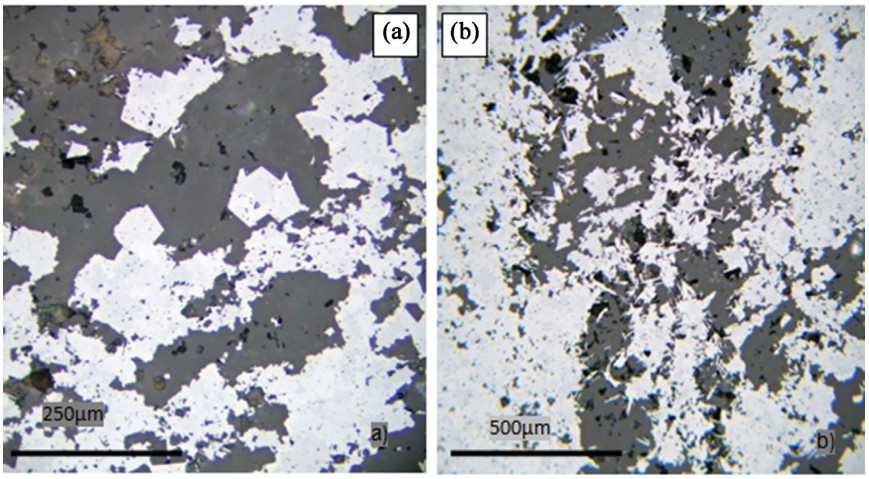

Figure 6. Reflected light microscopy of MZ008 showing (a) the presence of martite after oxidation of the magnetite and its relationship with the quartz (white). In (b) the weak development of hematite from the martite surface (in white). The quartz is grey.

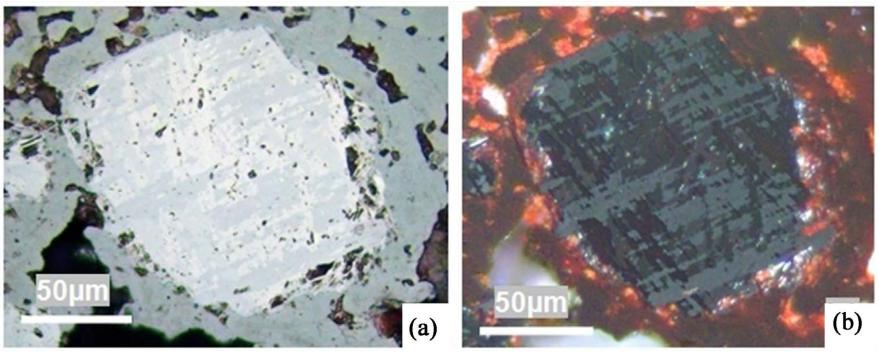

Figure 7. Microscopic observation in reflected and natural light of MZ017 in (a) and in polarised light in (b) showing the oxidation process from magnetite to martite. This oxidation leads to a lattice-like lamellar texture developing along the crystallographic plane of the magnetite shown in white or light grey in (a) and clearly visible in (b) because of its different optical orientations.

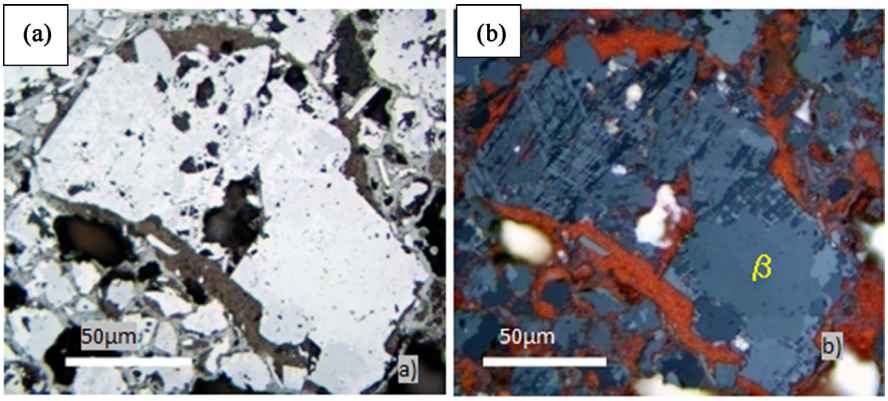

Figure 8. A pair of images from reflected light microscopy of MZ022 taken in (a) natural light and (b) polarised light illustrating deeply martitised magnetite crystals. The oxidation of the lattice-like martite developed along the crystallographic planes of the magnetite is discernible in white and/or light grey in (a), but clearly visible in polarized light in the upper left of the image in (b). The presence of a well-recrystallized martite (marked in yellow by the letter β) can also be seen in the lower right-hand part of the image in (b).

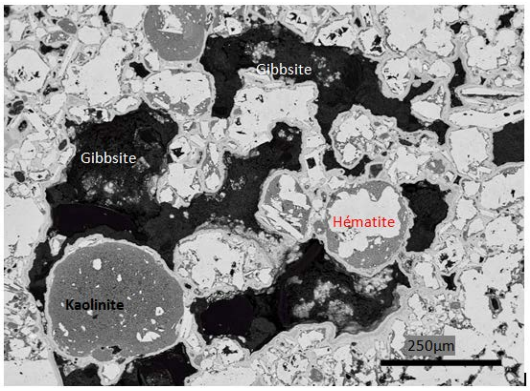

Figure 9. Microscopic observation of sample MZ022 from the scanning electron microscope illustrating the relationships between slightly ferruginous kaolinite with rounded elements (medium grey), gibbsite (dark grey) and concretion goethite (light grey) which are present all around the martite (white) and kaolinite rim. Hematite inclusions can also be seen in the kaolinite bodies.

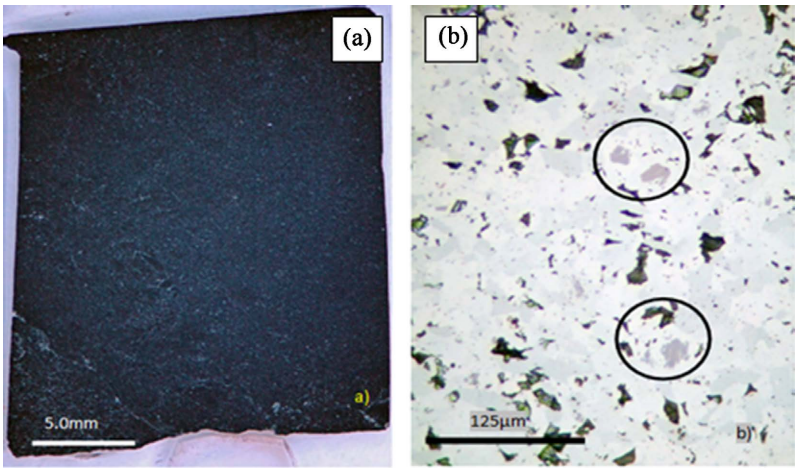

Figure 10. In (a): a photograph of a polished section of MZ024 illustrating the appearance of a sample consisting essentially of aggregates of recrystallized and porous martite. In (b) a microscopic observation in reflected light of a zone consisting largely of recrystallized martite, finely grained (white to light grey). We also note the presence of several cores of unoxidised magnetite (pink and circled).

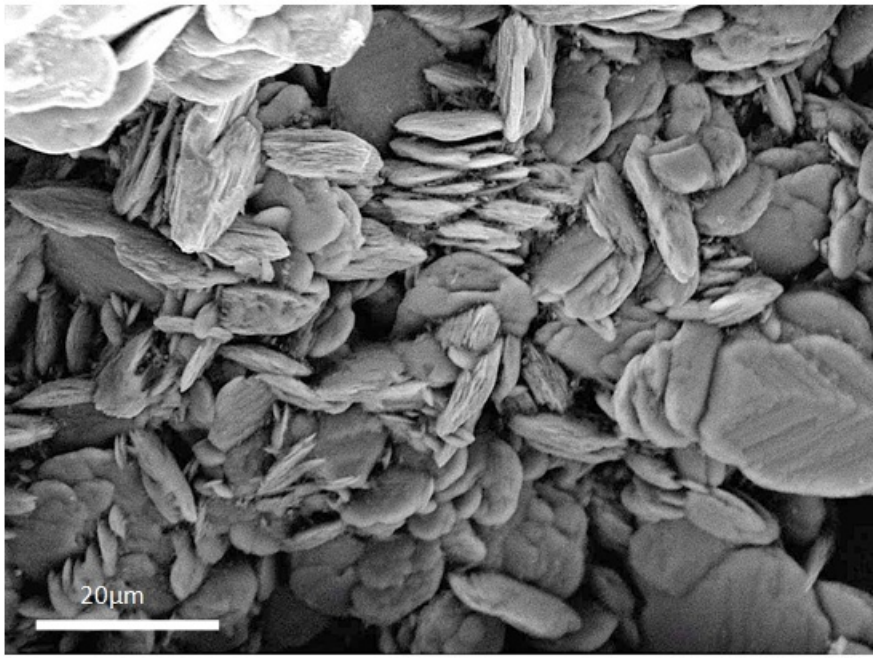

Figure 11. Microscopic observation of the MZ024 sample using a scanning electron microscope, illustrating the presence of the fine hematite crystals that have developed on the surface of the martite aggregates and are present in the cavities.

4.2. Drilling Samples

Several holes were drilled in the Zatua Hills area, including 4 holes selected in order to determine the depth of iron ore enrichment, alteration and the evolution of secondary minerals that could influence the quality of these iron ores.

4.2.1. Macroscopic Analysis

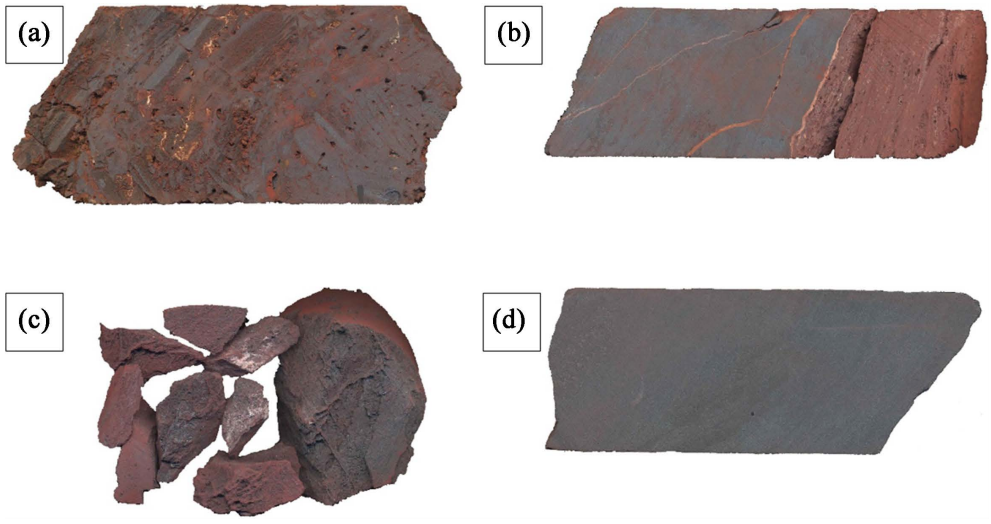

Figure 12. Borehole samples from the Zatua Hills: a hematitite with kaolinite and gibbsite (SMZ001 in (a)), a hydrated hematite with goethite (SMZ005 in (b)), a friable and fractured hematite (SMZ009 in (c)) and a finely grained hematite with laminations that are difficult to distinguish with the naked eye (MZ008 in (d)).

4.2.2. Microscopic Analysis

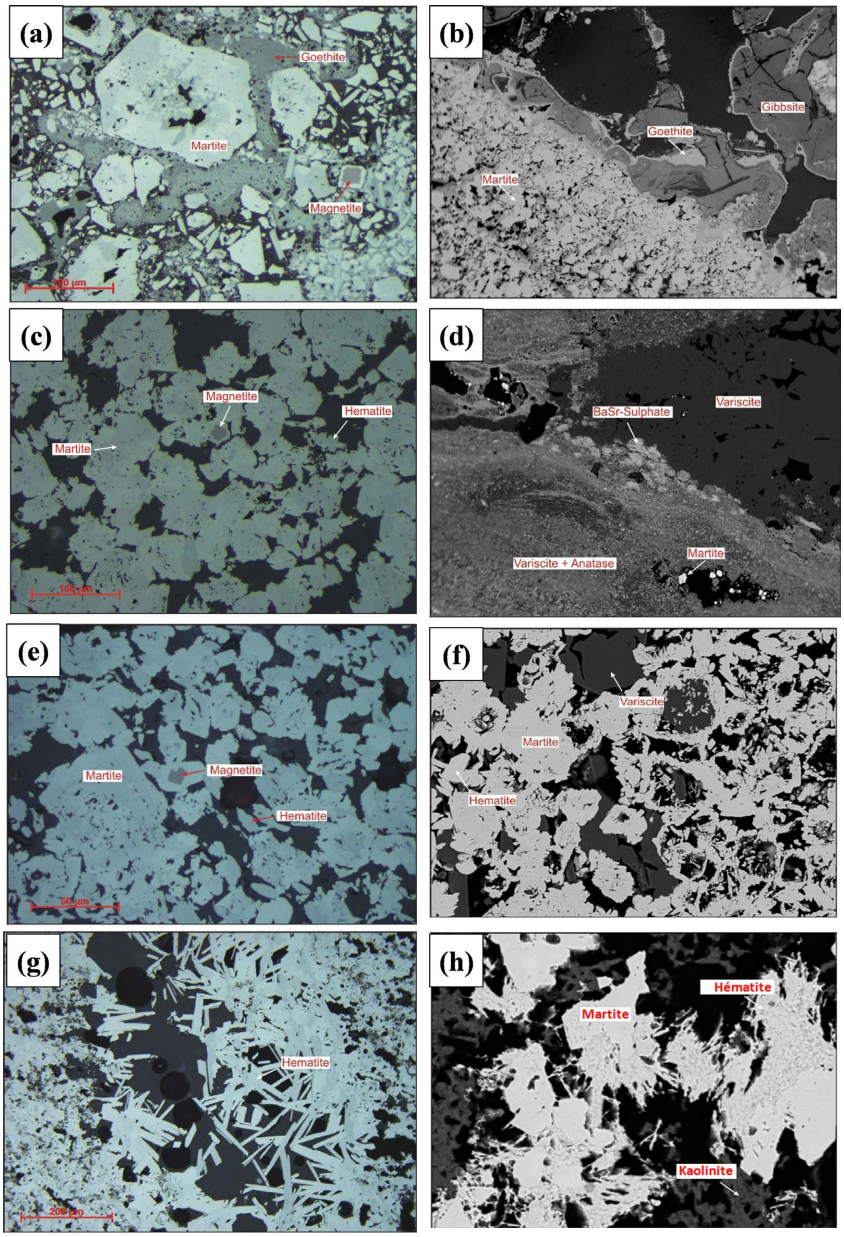

Figure 13. Microscopic observation showing: in (a) (optical microscope of SMZ001) the partial oxidation of martite (light grey) and its replacement by goethite with the presence of a low rate of magnetite (medium pinkish grey) and microplaty hematite. In (b) (SEM of SMZ001): the concordant and discordant crystals of goethite (medium grey) and gibbsite (dark grey) filling the fractures and cavities associated with the pores in the martite-rich laminations (light grey). In (c) (optical microscope of SMZ005): the same martite aggregates cemented by a low level of hematite and interstitial variscite (dark grey). We note the presence of magnetite at a low level (medium pinkish grey). In (d) (SEM of SMZ005): the complex appearance of the whitish clay layer consisting of the sample's reddish-brown variscite (dark grey) and anatase (medium grey). We also note the presence of the Ba and Sr sulphate deposition phase in the rock and the anatase phase alone without variscite filling the cavities in the sample. In (e) (light microscope of SMZ006): martite crystals (light grey) with relics of magnetite (medium pinkish grey) cemented by a small amount of microplaty hematite. Interstitial variscite is also present in the cavities (undifferentiated dark grey). In (f) (SEM of SMZ006): partially leached, porous martite (light grey on the right-hand side of the image) and interstitial variscite (dark grey) with low levels of microplaty hematite in the cavities between martite grains. In (g) (SEM of SMZ009): the presence of acicular hematite crystals developed in the pores. In (h) (SEM of SMZ009): porous aggregates of hematite hosting silica (light grey) which partially replaces the martite (light grey).

5. Discussion

5.1. Petrography

The various analysis carried out on surface and borehole samples in the Zatua Hills (**Figure 3** and **Figure 12**) have revealed that, both at surface and at depth, the same genetic processes that led to the enrichment of the BIFs in exploitable rich iron ore. These analyses clearly show that for BIFs samples whose quartz has been largely leached and enriched in iron, the other deleterious elements or iron impurities (Al, P and Si) are less represented in the samples (**Figure 9**, **Figure 13(b)** and **Figure 13(d)**). This leaching is possible along zones of weakness linked to rock joints, fractures and folding leading to the departure of primary quartz and the concentration of iron ores (magnetite, martite and hematite). Where the voids left by the departure of the primary silica are not filled, secondary hematite, goethite, gibbsite, kaolinite, cadwaladerite, strengite, variscite and other forms of ferruginous clay fill the pores as a matrix, consolidating the rock fragments (in the case of mineralised breccias). These secondary minerals are also the real sources of deleterious elements such as Si (residual silica and kaolinite), P (strengite-variscite solid solution), Al (gibbsite, cadwaladerite and kaolinite), Cl (cadwaladerite); and the hydration level of the rock.

All of these replacements took place through a succession of genetic processes that were sometimes cancelled out by other events. The supergene process is the last to be perceptible in the samples observed and through which meteoric waters are largely responsible for the transformation or leaching of the rock leading to its enrichment in iron (Morris, 1980, 1985, 2002; Harmsworth et al., 1990).

This observation remains as far as possible in favour of the modified supergene-hypogen process associated with metamorphism (Beukes et al., 2002; Gutzmer et al., 2006; Lascelles 2002, 2007), whereby hydrothermal solutions, waters from the deconvolution of rocks hydrated by retrograde metamorphism and meteoric waters played a major role in the leaching of silica and the enrichment of BIFs in exploitable rich iron ores. The presence of Ti in borehole samples (**Figure 13(d)**) clearly shows that it is associated with both phyllites and BIFs. Phyllites (chlorites, sericite schists) are considered to be low-temperature metamorphic rocks derived from the argillites found in this sedimentary basin. The affinity of titanium to this type of rock shows that the form of titanium oxide associated with it would be anatase, which corresponds to this type of low-temperature, low-pressure metamorphism.

5.2. Metalogeny of Zatua Hills BIFs

The samples selected for petrographic analysis helped us to put forward arguments concerning the magnetite-martite-hematite paragenesis, silica leaching, the development of microplaty hematite, the development of goethite and other secondary minerals considered to be deleterious to iron ores.

1) Magnetite-Martite-Hematite paragenesis

Referring to the macroscopic and microscopic observations of the surface and borehole samples in the preceding pages, we can see that the initial iron oxide in the BIFs of the Zatua Hills was magnetite, ideally ($Fe^{2+}Fe^{3+}{}_2O_4$) which was deeply oxidised to martite (Fe_2O_3) as expressed in the following equation (**Figure 4(b)**, **Figure 7(a)** and **Figure 7(b)**, **Figure 10(b)** and **Figure 13(a)**, **Figure 13(c)** and **Figure 13(e)**):

$$2Fe_3O_4 + 1/2\,O_2 \Rightarrow 3Fe_2O_3$$

The oxidation process began around the grains and along the fractures from which it progresses parallel to various directions of the crystallographic axes of the magnetite. This oxidation process leads to the development of martite aggregates in the form of lattice networks reflecting the positions of the magnetite crystallographic planes in relation to the oxygen cation planes observed in the magnetite cubic and hematite rhombohedral networks (**Figure 7(a)** and **Figure 7(b)**).

As the oxidation process begins, the lamellar martite crystals gradually enlarge and become more abundant until the remaining magnetite crystals are completely oxidised and replaced by martite aggregates. These martite lamellae and lattice structures are commonly preserved and serve as witnesses to confirm the presence of magnetite as a protore mineral (**Figure 7(a)** and **Figure 7(b)**).

Locally, small magnetite crystals survive within the cores of martite aggregates. The fine martite crystals produced during the oxidation process commonly form pseudomorphic substitutions of magnetite, preserving its detail in the primary microstructures (**Figure 4(b)**).

The oxidation process responsible for the martitisation of the magnetite in the Zatua Hills samples studied is deep and extensive; only traces of the unoxidised magnetite crystals are still visible in the samples (**Figure 4(b)**, **Figure 7(a)** and **Figure 7(b)**, **Figure 10(b)** and **Figure 13(a)**, **Figure 13(c)** and **Figure 13(e)**). Under low-temperature (near-surface) oxidation conditions, the oxidation products of the martite have lattice structures. They are, however, often present locally in the outcrops studied and, where they are present, they commonly show large crystals and interspersed lamellae (**Figure 7(a)** and **Figure 7(b)**). In many cases, the pseudomorphic martite consists of finely grained aggregates showing the early stages of recrystallization and grain development. In these cases, the martite particles are recrystallized and grain development processes are initiated in the conversion of martite lamellae to equidimensional crystals. These aggregates typically show a strong irregularity in the contours of the crystals formed, indicating a lack of crystallographic equilibrium.

The low degrees of recrystallization observed in most of the samples suggest that there was a slight increase in temperature at some stage after the oxidation process. These temperatures were, however, neither too high nor for a long pe-

riod to allow the martite recrystallization process to continue. One exception to this observation is the development of very elongated hematite crystals in this zone. This reflects the recrystallization of the finely grained martite along the small shear planes of the iron ore (**Figure 6(b)** and **Figure 13(f)-(h)**).

2) Silica leaching process and development of microplaty hematite

The textural evidence described in the petrographic section suggests that most of the BIFs samples in the suite studied consist of quartz bands and magnetite. These BIFs are considered to be prototypical iron ores and contain around 50% or less Fe_2O_3 with silica predominating. Leaching of quartz led to the development of pores in the rock, which still persist in some of the samples analysed. The presence of abundant pores increases permeability and provides a favourable space for the precipitation of secondary minerals.

The first stage in filling these pores with matrix constituents is the development of microplaty hematite. Typically, crystals of microplaty hematite form a core on the surface of the pseudomorphic martite and begin to grow.

These crystals are favourably oriented in the direction of leaching from the cavities, and the pores are then able to develop elongated or scale-like crystals of microplaty hematite, also known as specularites, on their outer surface (**Figure 6(b)** and **Figure 13(f)-(h)**).

The abundance and extent of these crystals in the rock varies from sample to others. In some samples, abundant, well-developed hematite crystals are found, while in others they are virtually absent. The development of these crystals contributes to the cementation of the pores in the martite-rich fraction.

The primary nature of the iron fragments and other forms of breccia is marked by the development of a low rate of microplaty hematite crystals developed in the matrix between the well mineralized fragments, thus preserving their morphologies.

The development of microplaty hematite crystals reflects the introduction into the system of a variable rate of additional iron leading to varying degrees of iron enrichment. Microplaty hematite is an important constituent of iron-rich ores, but virtually absent in iron-poor ores, and it probably develops with a slight increase in temperature, which is responsible for the early recrystallization of martite (Lascelles, 2007).

These types of hematite crystals are cemented by well-formed crystals of secondary hematite associated with goethite and other secondary minerals deposited later, and form a botryoidal or concretion texture inside the pores, but sometimes an acicular texture (**Figure 8**, **Figure 9** and **Figure 13(a)**).

Microplaty hematite is the result of a thorough leaching process of BIFs. This process is on the one hand supergene, marked by the oxidation of magnetite, by meteoric fluids and by the recrystallization of pre-existing martite; and on the other hand hypogene, marked by the precipitation of hematite from the oxidation of hydrothermal fluids (Powell et al., 1999; Lascelles, 2007) and the dehydration of goethite (Morris, 1985, 2002).

The supergene process and the dehydration of the goethite require oxidation, due

to alteration, followed by burial and Low Temperature Metamorphism (LTM).

3) Development process of goethite and other secondary minerals

It is true that secondary minerals are produced by precipitation in pores, fractures and other permeable zones under low-temperature, near-surface conditions. These minerals largely consist of goethite associated with secondary hematite, kaolinite, gibbsite, strengite-variscite solid solutions and cadwaladerite. The petrographic analyses presented in the previous sections have attempted to provide more details, but here we will attempt to give summaries.

The porous and permeable nature of many samples allows free circulation of aquifers and provides suitable sites for the precipitation of one or more secondary minerals. These minerals commonly show the development of fine bands, with botryoidal or concretionary textures, which indicate precipitation along the pores and lead to the formation of a hard crust. Unfortunately, these secondary minerals, notably goethite, kaolinite, gibbsite and the strengite-variscite solid solution serie, are the source of a significant proportion of the deleterious elements or impurities in the majority of samples.

The secondary minerals in these samples are marked by the composition of silicon (quartz or chert, goethite and kaolinite), aluminium (gibbsite, variscite, cadwaladerite, goethite and kaolinite) and phosphorus (variscite) in the analyses (Makuku et al., 2018).

a) Goethite

It has a ubiquitous phase, and is the most abundant of the secondary minerals in the samples processed. It is developed in the form of fine bands, with a botryoidal or concretional texture on the external surfaces of leached cavities, along fractures, in other permeable spaces in the rock and serves as a matrix of the rock cementing the rock fragments (case of breccias mentioned above).

In some cases, goethite appears to flood the rock, filling most of the pores. The very fine nature of the goethite bands indicates variations in the degree of crystallinity, levels of hydration of hematite or martite and impurities (Morris, 1980, 1985, 2002; Harmsworth et al., 1990).

The goethite inter-grows with the martite crystals in the samples and becomes problematic as its content increases. In addition to its water content, petrographic and geochemical analyses show that it contains a certain amount of Si and Al, as well as P (Makuku et al., 2023). A small percentage of Ti is also present. In some samples rich in Al and gibbsite, goethite can also contain Al and be classified as Al-goethite (**Figure 9**).

b) Secondary hematite

Secondary hematite is far less abundant than goethite among the minerals precipitated in the pores at the last phase (botryoidal or concretion textures). Where it is present, it is often associated in layers with goethite and, in a way, represents the dehydration product of goethite (**Figure 9**, **Figure 13(c)**, **Figure 13(g)**, **Figure 13(h)**).

Unlike the associated goethite, scanning electron microscope (SEM) analyses of this type of hematite show that it is close to the theoretical Fe_2O_3 composition, and is essentially free of the impurities associated with goethite.

c) Kaolinite

Kaolinite is present in very small quantities, but can vary in some samples where it occupies, alone or in association with other impurities, pores and fractures. It also shows an unusual mode of occurrence in which it is present as small rounded bodies that may be induced by goethite or other secondary minerals (**Figure 9** and **Figure 13(h)**).

Kaolinite commonly shows varying degrees of secondary ferruginization, marked by a reddish colour and thousands of hematite inclusions. Scanning Electron Microscope (SEM) analysis of kaolinite shows the presence of Si, Al and often a small amount of Fe. Kaolinite does not contain all the deleterious elements such as Si and Al, although its degree of crystallinity and/or water content is variable.

d) Gibbsite

Gibbsite shows the same pattern of occurrence as kaolinite, but remains the most common mineral. It occurs alone or in association with goethite and/or kaolinite (**Figure 9** and **Figure 13(b)**). SEM analysis shows that gibbsite consists mainly of Al, but its water content and degree of crystallinity are variable. Gibbsite is often a very late phase of precipitation and is located at the core of the goethite in the pores or at the center of the transgressive goethite in the fractures.

e) Anatase (Titane Oxide)

The presence of Ti in borehole samples clearly shows that it is associated with both phyllites and BIFs. Phyllites (chlorites, sericite schists) are considered to be the low-temperature metamorphic rocks derived from the argillites found in this sedimentary basin. The affinity of titanium to this type of rock shows that the form of titanium oxide associated with, it would be anatase, which corresponds to this type of low-temperature, low-pressure metamorphism (**Figure 13(d)**) (Makuku et al., 2023).

f) Strengite-Variscite solid solutions

Some samples analyzed in this zone show high phosphorus content, which is the highest possible found in associations of elements hosted by goethite. In most cases, the source of the high phosphorus content can be traced to the presence of strengite-variscite solid solution [ideally formulated: $FePO_4{\cdot}2H_2O$ - $AlPO_4{\cdot}2H_2O$]. The composition of these minerals is variable for Al-rich solid solutions associated with gibbsite. On the other hand, the iron-rich elements of the solid solution (strengite) are commonly present in zones devoid of Al-rich minerals. These minerals can contain between 38% and 55% P_2O_5 and their low level in the sample has enormous consequences for the metallurgical quality of the iron ore (Makuku et al., 2023).

g) Cadwaladerite and associated phases

Cadwaladerite [$AlCl(OH)_2 \cdot 4H_2O$] is the chlorine-rich mineral identified in various iron deposits, most notably in the West Zatua samples (**Figure 9**). This phase occurs as fine grains inter-growing with gibbsite and/or strengite-variscite solid solutions, but its composition is variable and reflects an amorphous mineral. It is possible that traces of cadwaladerite are also present in the goethite and probably in the clay minerals.

It has been observed that the presence of abnormal levels of P_2O_3 in the borehole samples is linked to fracture zones where the circulation of clay minerals is regular in association with phosphorous minerals, which circulation reflects a supergene process par excellence (Makuku et al., 2023).

6. Conclusion

All the samples collected on the Zatua Hills, both during the geological survey work and in the various boreholes drilled, show a broad family of BIFs whose iron-enrichment process classifies them as rich BIFs, poor BIFs, friable hematites, hard hematites, mineralised and unmineralized breccias, with metasediments (phyllades) as host rocks and certain dolerite intrusions.

The various petrographic analyses and metalogenic studies carried out on the samples collected on the Zatua Hills show:

- Hard BIFs, structurally made up of alternating bands of magnetite and/or hematite with those of quartz (silica), sometimes altered and interspersed with quartz veins. Goethite is visible in altered areas where the magnetite and/or hematite has been hydrated by circulating fluids;

- The hard or friable hematites show a high iron content, than in the BIFs, and consisting of laminations that are difficult to observe with the naked eye, the altered parts of which show the presence of goethite and other secondary minerals;

- Breccias, the result of the residual disintegration of both BIFs and hematites, found on the flanks of the Zatua Hills, which lead to unmineralized breccias and mineralized breccias respectively. The constituents of these breccias are either fragments of hematites or BIFs, or a mixture of these two types of rock cemented together by secondary hematite.

The analyses carried out on all the samples clearly show that magnetite (Fe_3O_4) was the most abundant iron oxide in the pre-existing iron formations. This magnetite was, however, oxidised to martite, with a lattice-like texture, before reaching the hematite stage at certain stages of deposition. These iron ores are sometimes subjected to brittle tectonics with opening in which the various Al, Al-P and Al-Fe-P phases precipitated as late vein fillings. These secondary minerals were precipitated to varying degrees within interstitial cavities leached between martite and hematite aggregates in botryoidal texture. These minerals are typically Al-rich, and consist of gibbsite and variscite-strengite solid solution series ($AlPO_4 \cdot 2H_2O$ and $FePO_4 \cdot 2H_2O$). This solid solution can have a chemical composition $(Al, Fe)PO_4 \cdot 2H_2O$ in which the proportions of Al and Fe can vary

significantly.

It should be noted that hematite and goethite inter-grow in the rock matrix, forming layers that overlap at various scales and develop a concretionary and/or botryoidal or reniform (grape cluster-shaped) texture that indicates their deposition in the pores.

The transition from magnetite to martite is thought to have taken place at low temperature, which could certainly be attributed to the effect of weak metamorphism, as evidenced by the irregular contours of the martite crystals observed microscopically, indicating that this recrystallization has not yet reached equilibrium conditions. This argument is also supported by the presence at depth of accessory minerals such as variscite and anatase, which are probably formed by precipitation from low-temperature supergene fluids under the rock's alteration conditions. Variscite is formed from the phosphorus-rich aquifer reacting with aluminium-rich (peraluminous) rocks under alteration conditions.

Anatase is a low-temperature form of rutile (TiO_2) and was probably formed under the same conditions as variscite. Titanium-rich fluids formed during the oxidation and alteration processes of titanium-rich oxides and silicates can precipitate anatase when Eh (redox) and pH conditions fall in the alteration profile.

Conflicts of Interest

The authors declare no conflicts of interest regarding the publication of this paper.

References

Allibone, A., Vargas, C., Mwandale, E., Kwibisa J., Jongens, R., Quick, S., Komarnisky, N., Fanning, M., Bird, F., MacKenzie, D., Turnbull, R., & Holliday, J. (2020). Orogenic Gold Deposits of the Kibali District. Neoarchean Moto Belt, Northeastern Democratic Republic of Congo. In R. H. Sillitoe, R. J. Goldfarb, F. Robert, & S. F. Simmons (Eds.), *Geology of the World's Major Gold Deposits and Provinces* (pp. 185-201). Society of Economic Geologists, Inc. https://doi.org/10.5382/SP.23.09

Beukes, N. J., Gutzmer, J., & Mukhopahyay, J. (2002). The Geology and Genesis of Highgrade Hematite Iron Ore Deposits. In *Iron Ore 2002* (pp. 23-29). The Australasian Institute of Mining and Metallurgy Publication Series 7/2002.

Bird, P. J. (2016). *Evolution of the Kibali Granite-Greenstone Belt, North East Democratic Republic of the Congo, and Controls on Gold Mineralisation at the Kibali Gold Deposit*. Unpublished Ph.D. Thesis, Kingston University, 307 p.

Borg, G., & Shacklet, R. M. (1997). The Tanzania and NE-Zaire Cratons. In M. J. de Wit, & L. D. Ashwal (Eds.), *Creenstone Belts* (pp. 608-619). Oxford University Press.

BRGM (Bureau de Recherches Géologiques et Minières) (1982). *A Geology and Mineral Map of Northeastern DRC Complied from by the BRGM (1980-1982) from a Field Survey in 1976 from Geological Maps Haut Zaire (Uele Area), Haut Zaïre (Ituri Area) at 1:500,000 Scale*.

Cahen, L., & Snelling, N. J. (1966). *The Geochronology of Equatorial Africa*. North-Holland Publishing Company.

Cahen, L., Snelling, N. J., Delhal, J., & Vail, J. R. (1984). *The Geochronology and Evolution of Africa*. Oxford Science Publishing, Clarendon Press, 512 p.

de Wit, M. J., & Linol, B. (2015). Precambrian Basement of the Congo Basin and Its Flanking Terrains. In M. J. de Wit, F. Guillocheau, & M. C. J. de Wit (Eds.), *Geology and Resource Potential of the Congo Basin* (pp. 19-37). Springer. https://doi.org/10.1007/978-3-642-29482-2_2

Gutzmer, J., Mukhopadhyay, J., Beukes, N. J., Pack, A., Hayashi, K., & Sharp, Z. D. (2006). Oxygen Isotope Composition of Hematite and Genesis of High-Grade BIF-Hosted Iron Ores. *Geological Society of America Memoirs, 198,* 257-268. https://doi.org/10.1130/2006.1198(15)

Harmsworth, R. A., Kneeshaw, M., Morris, Robinson, C. J., & Shrivastava, P. K. (1990). BIF-Derived Iron Ores of the Hamersley Province. In F. E. Hughes (Ed.), *Geology of the Mineral Deposits of Australia and Papua New Guinea* (pp. 617-642). Australasian Institute of Mining and Metallurgy.

Lascelles, D. F. (2002). A New Look at Old Rocks—An Alternative Model for the Origin of *in Situ* Iron Ore Deposits Derived from Banded Iron-Formation. In *Iron Ore 2002* (pp. 107-126). The Australasian Institute of Mining and Metallurgy Publication Series 7/2002.

Lascelles, D. F. (2007). Black Smokers and Density Currents: A Uniformitarian Model for the Genesis of Banded Iron-Formations. *Ore Geology Reviews, 32,* 381-411. https://doi.org/10.1016/j.oregeorev.2006.11.005

Lavreau, J. (1980). *Etude géologique du Zaïre septentrional. Génèse et évolution d'un segment lithosphérique archéen*. Unpublished Ph.D. Thesis, Université Libre de Bruxelles.

Lavreau, J. (1982). The Archaean and Lower Proterozoic of Central Africa. *Revista Brasileira de Geosciências, 12,* 187-192.

Lavreau, J. (1984). Vein and Stratabound Gold Deposits of Northern Zaïre. *Mineralium Deposita, 19,* 158-165. https://doi.org/10.1007/BF00204680

Lavreau, J., & Ledent, D. (1975). Etablissement du cadre géochronologique du Kibalien. *Annales de la Société Géologique de Belgique, 98,* 197-212.

Lavreau, J., & Navez, J. (1982). The Geochemistry of the Archaean Greenstones of Northern Zaïre. I. Analytical Results and Statistics. Rapp.ann. 1981-1982, Mus. roy. Afr. centr., Dépt. Géol. Min.Tervuren: 101-104.

Makuku, L. M., Ongendangenda, A., Kanda, N. V., & Kombie, A. P. F. (2018). Caractéristiques géologiques et pétrographiques des BIFs des Monts Zatua, Nord-Est de la RDC. *Revue de Congo Sciences, 6,* 141.

Makuku, L. M., Wetshondo, O. D., Kanda, N. V., Nzambe, K. K., & Ongendangenda, T. A. (2023). Geochemical Signature and Metalogeny of BIFs and Associated Iron Ore of Zatua Hills, Haut-Uele Province (DR Congo). *Journal of Geoscience and Environment Protection, 11,* 201-217. https://doi.org/10.4236/gep.2023.1110014

Morris, R. C. (1980). A Textural and Mineralogical Study of the Relationship of Iron Ore to Banded Iron-Formation in the Hamersley Iron Province of Western Australia. *Economic Geology, 75,* 184-209. https://doi.org/10.2113/gsecongeo.75.2.184

Morris, R. C. (1985). Genesis of Iron Ore in Banded Iron-Formation by Supergene and Supergene-Metamorphic Processes—A Conceptual Model. In K. H. Wolf (Ed.), *Handbook of Strata-Bound and Stratiform Ore Deposits* (pp. 73-235). Elsevier. https://doi.org/10.1016/B978-0-444-42497-6.50006-0

Morris, R. C. (2002). *Iron Ore Genesis And Post-Ore Metasomatism at Mount Tom Price, Iron Ore 2002: Perth, Australia* (pp. 1-13). The Australasian Institute of Mining and Metallurgy Publication Series 7/2002.

Powell, C. M., Oliver, N. H. S., Li, Z. X., Martin, D. M., & Ronaszeki, J. (1999). Synorogenic Hydrothermal Origin for Giant Hamersley Iron Oxide Ore Bodies. *Geology, 27,* 175-178. https://doi.org/10.1130/0091-7613(1999)027<0175:SHOFGH>2.3.CO;2